*Aditya Rio Prabowo[1*], Toeri Fathuddin Yusuf[1], Prayoga Wira Adie[1,2], Nurul Muhayat[1], Iwan Istanto[1], Tuswan Tuswan[3], Achmad Zubaydi[4], Teguh Muttaqie[5], Quang Thang Do[6], Martin Jurkovič[7]*

# ENGINEERED NOVEL-MECHANICAL DESIGN AND PERFORMANCE ASSESSMENT OF STIFFENED PLATES AGAINST BALLISTIC LOADING

# NOVI INŽENJERSKI MEHANIČKI DIZAJN I OCENA PERFORMANSI UKRUĆENIH PLOČA PROTIV-BALISTIČKOG UDARA

Originalni naučni rad / Original scientific paper
Rad primljen / Paper received: 11.03.2025
https://doi.org/10.69644/ivk-2025-01-0089

Adresa autora / Author's address:
[1)] Department of Mechanical Engineering, Universitas Sebelas Maret, Surakarta, Indonesia *email: aditya@ft.uns.ac.id
A.R. Prabowo https://orcid.org/0000-0001-5217-5943
N. Muhayat https://orcid.org/0000-0002-1086-7826
I. Istanto https://orcid.org/0009-0009-9037-4375
[2)] Laboratory of Design and Computational Mechanics, Faculty of Engineering, Universitas Sebelas Maret, Surakarta, Indonesia
[3)] Department of Naval Architecture, Universitas Diponegoro, Semarang, Indonesia T. Tuswan https://orcid.org/0000-0002-0314-2616
[4)] Department of Naval Architecture, Institut Teknologi Sepuluh Nopember, Surabaya, Indonesia
[5)] Research Center of Testing Technology and Standard, National Research and Innovation Agency (BRIN), Tangerang, Indonesia
T. Muttaqie https://orcid.org/0000-0002-8850-8313
[6)] Department of Naval Architecture and Ocean Engineering, Nha Trang University, Nha Trang, Viet Nam
Q.T. Do https://orcid.org/0000-0002-4232-9563
[7)] Faculty of Operation and Economics of Transport and Communications, University of Žilina, Žilina, Slovakia
M. Jurkovič https://orcid.org/0000-0001-7673-1350

**Keywords**
- ballistic impact
- stiffener
- residual velocity
- material selection
- finite element analysis

**Ključne reči**
- balistički udar
- ukrućivač
- rezidualna brzina
- izbor materijala
- analiza konačnim elementima

*Abstract*

*This study shows a numerical analysis of the ballistic characteristic of a bullet on a targeted stiffened plate. The numerical analysis compares the structural strength of the target plate with stiffener variations of I, L, T, Y, and X types with various material variations of Al 6061-T651, Al 6082-T6, Weldox 460E, and Armox 500T. Numerical simulations are performed at a squared stiffened target plate at projectile impact velocity of 341-863 m/s using ABAQUS/ Explicit® with the Johnson-Cook material model. The initial validation is successfully achieved by comparing the residual velocity values between the current study and the previous experiment. Simulation results demonstrate that incorporating an I stiffener significantly enhances ballistic resistance, with performance varying based on material types. Weldox 460E combined with an I stiffener exhibits the best ballistic resistance performance. The study highlights the importance of optimising stiffener design and material selection to maximise ballistic protection performance.*

*Izvod*

*U radu je predstavljena numerička analiza balističkih karakteristika projektila sa ukrućenom pločom kao metom. U numeričkoj analizi se poredi čvrstoća konstrukcija ploče-mete raznih tipova ukrućenja I, L, T, Y i X i različitih materijala Al 6061-T651, Al 6082-T6, Weldox 460E i Armox 500T. Numeričke simulacije su izvedene sa kvadratnom ukrućenom pločom-metom pri udarnoj brzini projektila od 341-863 m/s primenom ABAQUS/Explicit® sa Džonson-Kuk modelom materijala. Početna procena je uspešno obavljena upoređivanjem vrednosti rezidualne brzine prethodnog eksperimenta i rezultata u ovom radu. Rezultati simulacije pokazuju da se uvođenjem I ukrućivača značajno povećava balistička otpornost, gde se performanse menjaju zavisno od tipa materijala. Weldox 460E materijal u kombinaciji sa I ukrućivačem pokazuje najbolje osobine balističke otpornosti. U radu se naglašavaju značaji optimizacije u dizajnu ukrućivača i izbora materijala, radi postizanja maksimalnih performansi balističke otpornosti i zaštite.*

## INTRODUCTION

Ballistic penetration resistance is critical in designing structural systems to withstand high-speed impacts, particularly for small arms such as pistols, submachine guns, and assault rifles, /1/. The defence industry places significant importance on understanding the behaviour of structures under ballistic impact to enhance military equipment and minimise losses during combat. Key design requirements for such structures include high ductility and mobility which demand lightweight materials without compromising structural integrity, /2/. The structural configuration of ballistic targets plays a crucial role in their resistance to penetration. Target structures can be strengthened by incorporating stiffeners which have been shown to enhance impact resistance significantly, /3/.

Stiffened plates are commonly used in aircraft, ships, and civil structures due to their superior buckling resistance under blast loading. While their behaviour under static loads is understood, extensive research in the past decade has focused on their response to uniform and localised blast load conditions /4, 5/. The stiffener type and arrangement are key in determining how resistant stiffened steel plates behave under ballistic impact. Numerous studies demonstrate that stiffener size, shape and configuration substantially affect stiffened steel plate resistance and dynamic response under blast load /6/. Moreover, the failure modes of stiffened plates under blast loads include large plastic deformation, partial plate damage, tensile tearing at the boundaries, and shear failure, all strongly influenced by the characteristics and configurations of the stiffeners. The position and arrangement of stiffeners affect these failure modes, and new sub-modes, such as partial tearing and rupture, have also been identified /7/. Moreover, stiffener type, number, and size significantly impact the energy absorption ratio of the stiffened plate, highlighting their critical role in energy dissipation during impact, /8, 9/.

The finite element method (FEM) has become an essential tool, complementing experimental results with numerical simulations. As noted in /10/, simulation offers the flexibility to explore hypothetical situations with minimal resources, accelerating the design and evaluation process. Widely used FEM tools, such as Abaqus® and LS-DYNA®, are employed to model and simulate impact scenarios on stiffened plates /11-14/. Nonlinear finite element study of ballistic phenomena may lead to safer and more affordable design, /15/. In these simulations, the Johnson-Cook (JC) model is commonly applied to accurately express the material behaviour under high strain rates and elevated temperature, /16, 17/.

Over the past decades, extensive studies have been performed on unstiffened target plates of various sizes and materials subjected to low-velocity impact loading, such as circular and square plates, /18, 19/. Investigations have been conducted into the impacts of boundary conditions, the indenter's mass and velocity, plate material and its shape /20-22/. However, stiffened and unstiffened plates fundamentally differ, complicating the penetration physical effects /23/. Several previous investigations have been conducted on the ballistic impact of stiffened panels, both numerical and experimental tests. By examining the impact point-stiffener configuration relationship, /24/, it is found that projectile attitude variation impacts target plate failure mode. In /25-28/ the researchers conducted low-velocity impact tests on stiffened panels under various stiffener spacing and material thickness, demonstrating the distinct effects of geometry on impact resistance. Large-scale investigations by Wang et al. /29/ on unstiffened and stiffened 921A steel target stiffened plates under truncated ogive projectiles examined the need to include Lode angle and stress triaxiality in the fracture criterion. Other studies on the low-velocity impact behaviour of T-shaped stiffened plate for ship structures under low-velocity impact were studied in /30/. Moreover, other stiffener configurations, such as double, cross, double cross, and U-shaped stiffener configurations, are subjected to blast loading, /31-33/.

Previous studies have provided a comprehensive understanding of the impact response of relatively thin, stiffened steels, primarily by employing modelling and analysis techniques for ballistic impacts. However, these studies have predominantly focused on specific stiffener configurations and material types, leaving gaps in knowledge regarding the broader range of design possibilities. Therefore, further investigation is required to explore the behaviour of stiffened steel plates under varying stiffener arrangements, geometric design, and alternative material selection. This current study numerically investigates the ballistic impact on stiffened steel plates using various stiffener configurations and material types by using FEM software. Benchmark tests compare previous experimental tests conducted by /34/ which focus on the ballistic impact tests involving target plates struck by ogive-nose steel rods under normal impact conditions.

## REFERENCE PROFILE

This research employs FEM software, building upon the experimental study conducted in /34/. The previous research focused on the energy absorption of aluminium plates subjected to ballistic impact, analysing the resulting plate deformations and residual velocities of projectiles. To ensure validity, the present study compares the FEM simulation results for residual projectile velocity and deformation contours with the experimental findings in /34/.

The FEM analysis in this study utilised the ABAQUS® software, adopting the same material properties and geometric configurations as those used in the earlier experimental study for consistency and validation. The projectile employed in the simulation features an ogive-nose geometry with a head radius of 3.0 calibre, a length of 67.5 mm, a diameter of 12.9 mm, and mass of 82 g. The target plate is a square Al 6061-T651 aluminium plate with dimensions of 304 mm × 304 mm and thickness of 26.3 mm. In this study, the initial velocity is placed at the reference point (RP) in the centre of the rear end of the projectile. The bottom side of the target plate is defined as fixed by constrained displacement and rotational DOF on that side. The mesh size for the FEM model is refined to 0.01 mm in the non-impact zone and 0.001 mm in the impact zone to capture localised effects accurately.

The study simulated nine variations of initial projectile velocities, with results summarised in Table 1 as residual velocities. Figure 1 compares the deformation contours of the target plates obtained from FEM simulations with those from experimental study across various initial velocities. The agreement between FEM results and experimental data is strong, with a maximum error of 2.99 %. It indicates the reliability of the FEM approach in replicating the ballistic impact behaviour of aluminium plates, further validating the model and methodology employed.

Table 1. Validation tests between the present study and experimental results.

| Initial impact velocity (m/s) | Residual velocity (m/s) | | Error (%) |
|---|---|---|---|
| | Experiment, /34/ | Numerical test (present study) | |
| 341 | 164 | 168.9 | 2.99 |
| 396 | 266 | 262.7 | 1.24 |
| 454 | 347 | 343.8 | 0.92 |
| 508 | 415 | 412.3 | 0.65 |
| 565 | 482 | 481.0 | 0.21 |
| 630 | 555 | 555.8 | 0.14 |
| 633 | 561 | 560.7 | 0.05 |
| 730 | 665 | 668.3 | 0.50 |
| 863 | 802 | 811.3 | 1.16 |

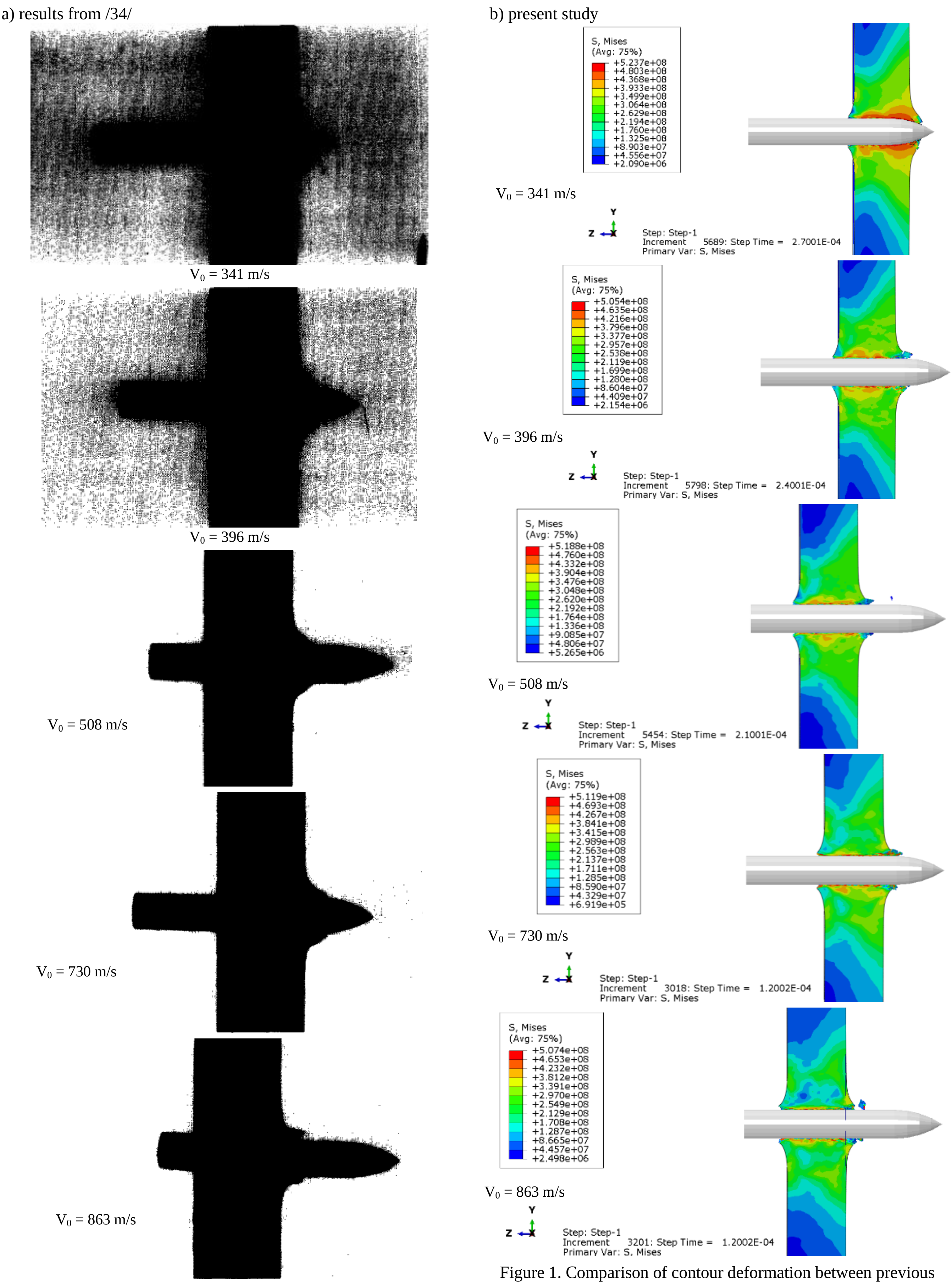


Figure 1. Comparison of contour deformation between previous research and current study.

## MESH CONVERGENCE STUDY

A mesh convergence analysis is performed to determine an optimal mesh size that balances computational efficiency with simulation accuracy. Using a coarser mesh can lead to inaccurate results, while an excellent mesh significantly increases computation time without substantial gains in accuracy. Conducting a mesh convergence analysis ensures that the FEM model provides reliable results while minimising computational overhead. This analysis was conducted before the parametric study to establish a stable and efficient mesh configuration.

The convergence analysis involves comparing residual velocity results at varying mesh sizes. As shown in Fig. 2, convergence was observed at a mesh size range of 0.0025-0.004 mm in the contact zone of the target plate. The FEM model employs trilinear displacement and temperature settings, with the target plate model using an 8-node thermally connected brick element. A mesh size of 0.01 mm is applied for the non-impact zone, resulting in 26 elements through the plate thickness. Based on the convergence analysis, a mesh size of 0.0025 mm is selected for the impact zone, as depicted in Fig. 3. This choice balances accuracy and computational efficiency, ensuring stable and relevant simulation results for subsequent parametric studies.

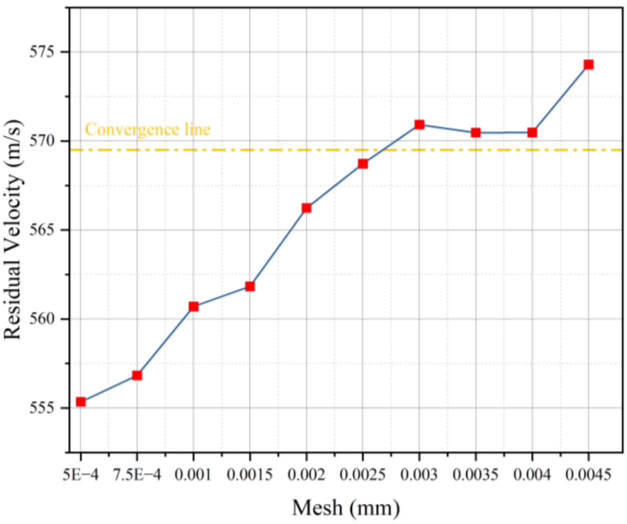


Figure 2. Mesh convergence test of residual velocity results.

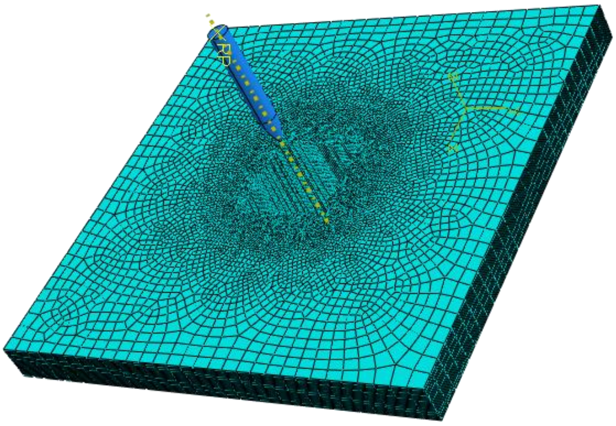

Figure 3. Computational mesh model of targeted stiffened plate.

## GEOMETRICAL MODEL

The simulation in this study comprises two primary components. The projectile, illustrated in Fig. 4a, features a round head with a radius of 3.0 calibre and a mass of 82 g, and is modelled as an analytically stiff body. This assumption ensures the projectile remains rigid during impact, isolating the deformation analysis to the target plate. The target plate, depicted in Fig. 4b, is modelled as a deformable solid with a square beam configuration. Six variations of the target plate are analysed to investigate the structural performance under ballistic impact. Five of these variations incorporate additional stiffeners designed in distinct geometrical shapes: I, L, T, Y, and X, as shown in Fig. 5. Each stiffener configuration is developed to evaluate its influence on the structural response and performance of the target plate under impact.

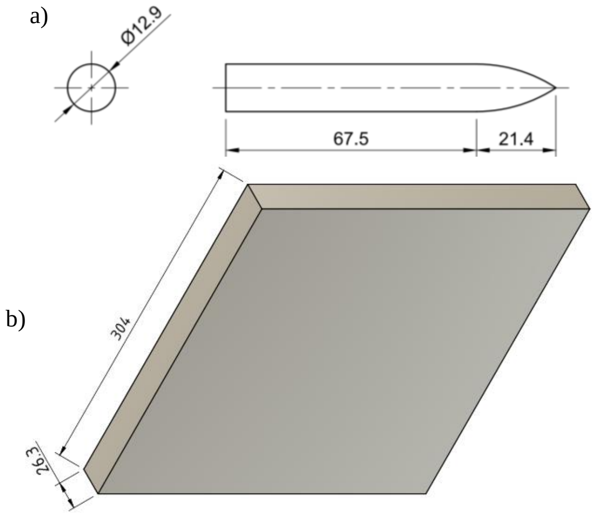


Figure 4. Geometry of: a) 3.0 circle-radius-head projectile; b) targeted plate.

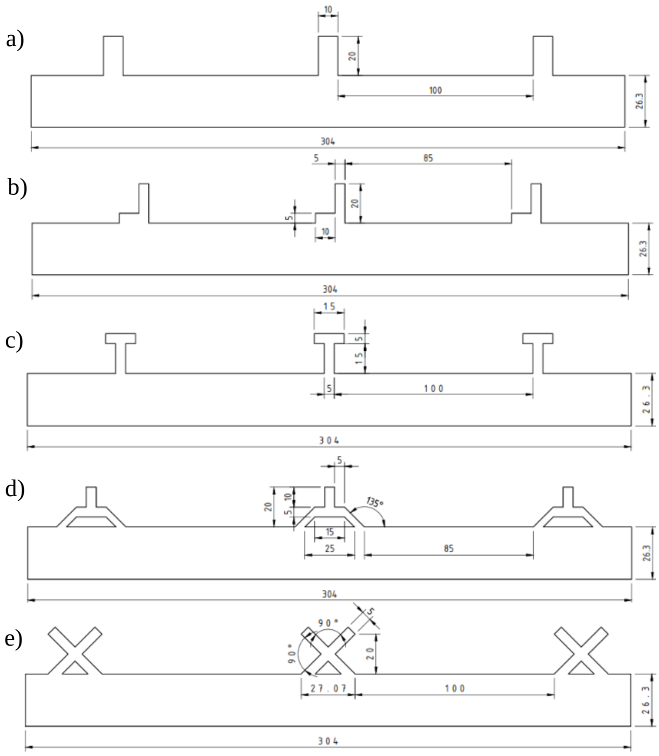


Figure 5. Stiffener geometry types: a) I; b) L; c) T; d) Y; and e) X.

## JOHNSON-COOK MATERIAL PROPERTIES

This study considers four materials for ballistic applications. Al 6061-T651 exhibits significant potential for military use due to its balance of strength, relatively low cost, and high-impact resistance, /35/. Al 6082-T6 is widely employed in artillery, defence vehicles, and aircraft structures owing to its favourable strength-to-weight ratio and corrosion resistance, /36/. Weldox 460E steel plates are frequently utilised in military applications for their robust projectile impact resistance, /21/. Meanwhile, Armox 500T steel is designed to protect against bullet penetration in ballistic scenarios /37/. Under high-speed impact, material behaviour is governed by strain rate and temperature effects. In this research, the target plate is modelled using the Johnson-Cook (JC) constitutive equation. The relevant JC material parameters for the target plate are listed in Table 2. The JC model describes the von Mises stress ($\bar{\sigma}$) as a function of equivalent plastic strain ($\bar{\varepsilon}^{pl}$), equivalent plastic strain rate ($\dot{\bar{\varepsilon}}^{pl}$), and temperature ($T$), as seen in Eq.(1), /38/,

$$\bar{\sigma} = (A + B(\bar{\varepsilon}^{pl})^n)/1 + C\ln(\dot{\bar{\varepsilon}}^{pl}/\dot{\bar{\varepsilon}}_0^{pl}))/(1 - T^{*m}) \,. \quad (1)$$

Based on Eq.(1), $A$, $B$, and $m$ are constants, $n$ is the strain hardening exponent, $\dot{\bar{\varepsilon}}^{pl}/\dot{\bar{\varepsilon}}_0^{pl}$ is the normalised plastic strain rate equivalent (usually normalised to 1.0 s$^{-1}$), and homologous temperature ($T^*$) is calculated using Eq.(2), where $T_0$ is initial temperature, $T$ is the deformation temperature, and $T_{melt}$ is melting temperature.

$$T^* = (T - T_0)/(T_{melt} - T_0) \;\; \text{for} \;\; T_0 < T < T_{melt} \,. \quad (2)$$

Table 2. Comparison of material properties of targeted plates, /39/.

| Material properties | Al 6061-T651 | Al 6082-T6 | Weldox 460E | Armox 500T |
|---|---|---|---|---|
| Density, $\rho$ (kg/m$^3$) | 2750 | 2700 | 7850 | 7850 |
| Poisson's ratio, $\nu$ | 0.3 | 0.3 | 0.33 | 0.33 |
| Young's modulus, $E$ (GPa) | 69 | 70 | 200 | 201 |
| Expansion coefficient | 2.10E-05 | 2.10E-05 | 1.17E-05 | 1.15E-05 |
| Initial yield stress, $A$ (MPa) | 324 | 201.55 | 490 | 1372.488 |
| Strain hardening coefficient, $B$ (MPa) | 144 | 250.87 | 807 | 835.022 |
| Strain hardening exponent, $n$ | 0.42 | 0.206 | 0.73 | 0.2467 |
| Strain sensitivity coefficient, $C$ | 0.002 | 0.00977 | 0.012 | 0.0617 |
| Thermal softening constant, $m$ | 1.34 | 1.31 | 0.94 | 0.84 |
| Reference strain rate ($\dot{\varepsilon}$) | 1 | 0.001 | 0.0005 | 1 |
| Melting temperature, $\theta_{melting}$ (K) | 600 | 855 | 1800 | 1800 |
| Transition temperature, $\theta_{transition}$ (K) | 50 | 293 | 293 | 293 |
| Specific heat, $C_p$ (J/kgK) | 900 | 900 | 452 | 455 |
| JC damage material constant, $D_1$ | -0.77 | 0.0164 | 0.0705 | 0.9 |
| JC damage material constant, $D_2$ | 1.45 | 2.245 | 1.732 | 0.04289 |
| JC damage material constant, $D_3$ | 0.47 | -2.798 | -0.54 | 2.1521 |
| JC damage material constant, $D_4$ | 0 | 0.007 | 0.147 | -2.7575 |
| JC damage material constant, $D_5$ | 1.6 | 3.65 | 0 | -0.0066 |

The JC model defines the yield stress ($A$), strain hardening constants ($B$ and $m$), elasticity modulus ($E$), and Poisson's ratio ($\nu$). Equation (3) defines equivalent plastic strain at the onset of damage in the JC model,

$$\bar{\varepsilon}_f^{pl}\left(\frac{\sigma}{\bar{\sigma}}, \dot{\bar{\varepsilon}}_f^{pl}, T^*\right) = \left[D_1 + D_2 \exp\left(D_3 \frac{\sigma_m}{\bar{\sigma}}\right)\right]\left[1 + D_4 \ln \frac{\dot{\bar{\varepsilon}}^{pl}}{\dot{\bar{\varepsilon}}_0^{pl}}\right] \times \times [1 + D_5 T^*] \,, \quad (3)$$

where: $D_1$ to $D_5$ are material parameters obtained based on different mechanical tests; $D_1$, $D_2$, and $D_3$ are stress triaxial parameters; $D_4$ is a strain rate-dependent damage parameter; $D_5$ is a temperature-dependent strain parameter; $\sigma_m/\bar{\sigma}$ is a stress triaxial ratio; $\sigma_m$ is the average stress.

## RESULTS AND DISCUSSION

This study conducted a numerical analysis to determine the projectile's residual velocity, calculated from its initial velocity at impact until it fully penetrates the target plate /39-48/. Additionally, impact outlines are presented to illustrate stress and strain distributions within the target. The plastic strain values are specifically examined to highlight permanent deformations resulting from ballistic impact.

## RESPONSE OF BALLISTIC IMPACT ON VARIOUS STIFFENER DESIGNS

Figure 6 compares the residual velocity of projectiles impacting target plates with five different stiffener configurations, namely I, L, T, Y, and X stiffeners, across a range of initial velocities. The result shows that as initial velocity increases, the residual velocity also increases for all configurations, indicating that higher incoming energy leads to higher exit velocities. Nevertheless, clear distinctions emerge among stiffener types due to their energy absorption capabilities and consequent velocity reduction. It can be found that the I stiffener consistently exhibits the most significant decrease in projectile velocity at comparable initial velocities. At 396 m/s, the I stiffener absorbs 3828.04 J of energy and reduces the projectile's velocity by 49.54 %, the highest among stiffener variants. This superior performance implies that the I stiffener design offers enhanced structural rigidity and an improved capacity for dissipating impact energy.

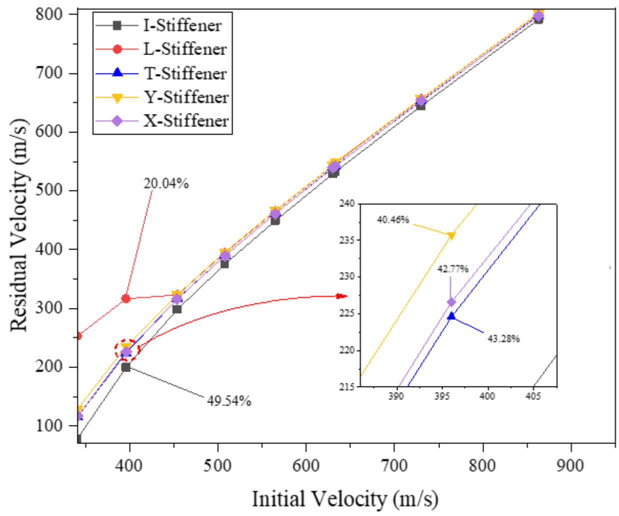


Figure 6. Residual velocity at different stiffener models.

Moreover, the L stiffener yields the highest residual velocity for a given initial velocity, reflecting the least efficient energy absorption. At an initial velocity of 396 m/s, it absorbs only 1777.64 J, amounting to a velocity reduction of just 20.04 %. Consequently, the L stiffener is less effective in mitigating projectile penetration than other stiffener models. The T, Y, and X stiffeners generally demonstrate moderate energy absorption capabilities, with outcomes between the I and L stiffeners.

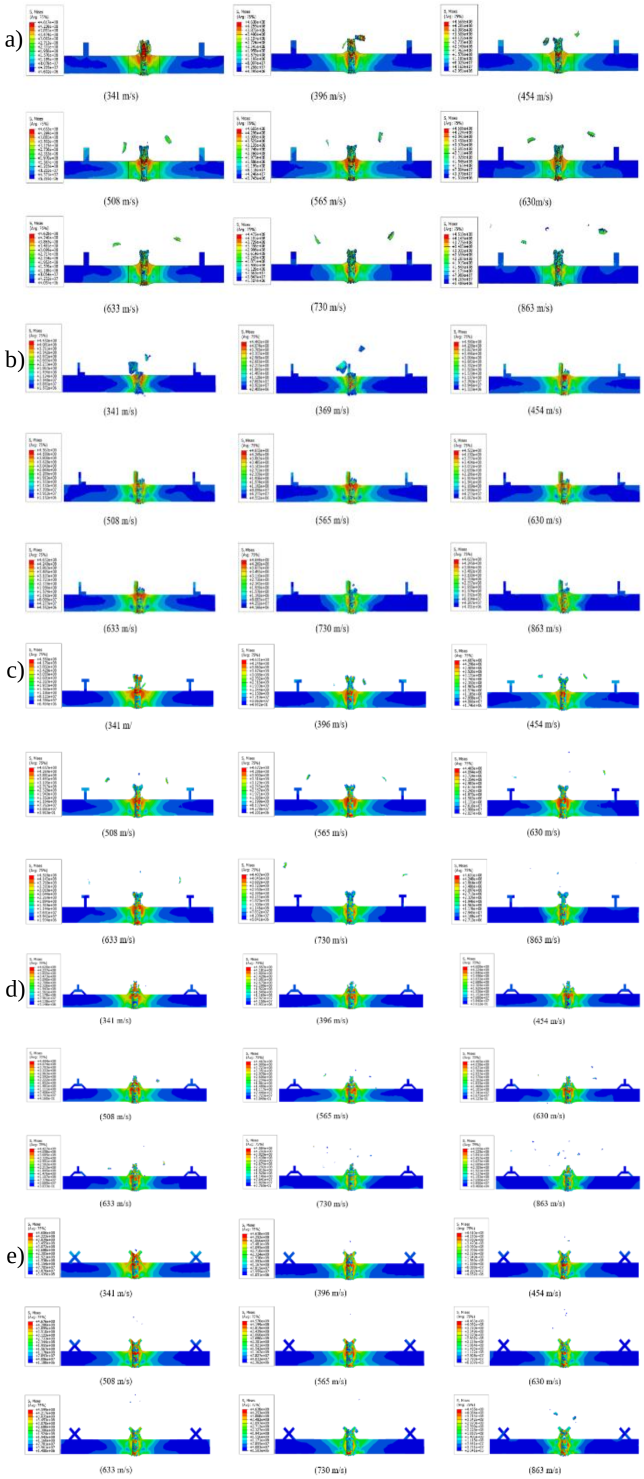

Figure 7. Stress contour of target plate with stiffeners: a) I; b) L; c) T; d) Y; and e) X.

Figure 7 presents stress contours corresponding to each stiffener configuration (I, L, T, Y, and X) over projectile impact velocities from 341 m/s to 863 m/s. The maximum stress is observed near the direct impact zone, where the projectile makes contact with the plate. With an increase in impact velocity (e.g., exceeding 630 m/s), the stress distribution from the impact centre becomes more extensive, resulting in larger areas of the plate experiencing elevated stress levels. At increased velocities, fragments of plate material and projectile debris become more evident, indicating enhanced damage and plastic deformation. At reduced velocities, stress remains localised around the impact point, resulting in smaller permanent deformations. As velocity increases (e.g., 730 m/s and above), the plate experiences elevated levels of plastic deformation, occasionally resulting in spallation and the detachment of material fragments from the rear side. Plates exhibiting a more uniform stress distribution, especially the I stiffener and certain features of the X stiffener, are associated with enhanced energy absorption and decreased residual projectile velocity due to their effective load distribution during impact. In contrast, configurations such as the L stiffener intensify stress concentrations, thereby reducing the plate's ability to dissipate impact energy and resulting in an increased residual velocity of the projectile.

The plastic strain contours of the target plate under projectile impacts in each of the five stiffener configurations are depicted in Fig. 8. The impacts range from approximately 341 m/s to 863 m/s. The regions of greatest plastic strain are consistently observed near the site of projectile contact. The direct kinetic energy transfer into the plate results in the most severe deformation in this area. These zones of intense strain tend to expand and penetrate deeper into the plate thickness as the impact velocity increases, indicating more significant overall damage. The I stiffener's high energy absorption capacity is demonstrated by plastic strain contours in Fig. 8, which suggest that deformation is directed along its height, resulting in a broader yet more uniform strain distribution. Conversely, the L stiffener's corner geometry concentrates strain at higher velocities, resulting in less efficient load distribution and higher residual projectile velocities. As observed in other analyses, the I and Y stiffener configurations effectively disperse high-strain zones more than the L stiffener, consistent with their relatively higher energy absorption and lower residual projectile velocities.

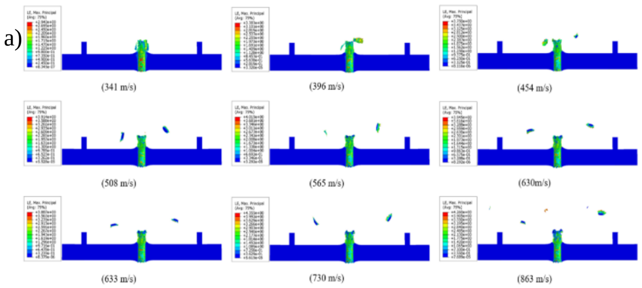

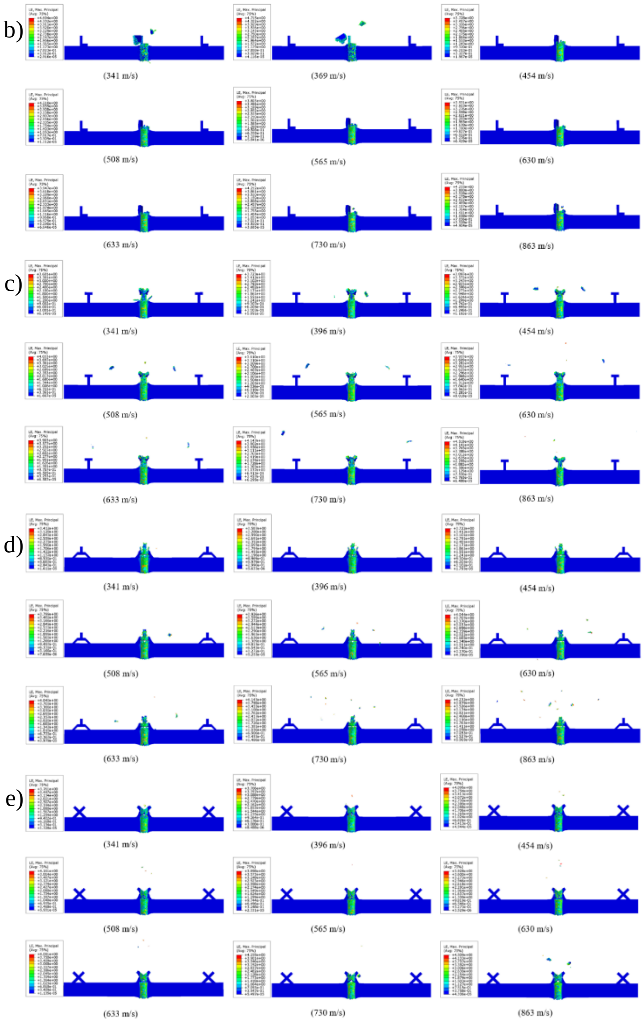


Figure 8. Strain contour of target plate with different stiffeners: a) I; b) L; c) T; d) Y; and e) X.

## RESIDUAL VELOCITY TRENDLINE ON VARIOUS STIFFENER DESIGNS

Figure 9 presents the residual versus initial velocity for each stiffener type and their respective polynomial trendlines. All five configurations generally show increasing residual velocity as the projectile's initial velocity rises, indicating that higher impact speeds result in greater energy carry-through after perforation. However, clear distinctions emerge in how effectively each stiffener mitigates projectile speed. It can be found that I stiffener in Fig. 9a exhibits the lowest residual velocity over the same range of initial velocities, aligning with its stronger energy absorption capabilities. By contrast, the L stiffener depicted in Fig. 9b shows a noticeably higher residual velocity, reflecting poorer ballistic resistance. The T, Y, and X stiffeners generally plot between these two extremes, with the X stiffener often trending closer to the I-stiffener in reducing projectile speed. These trendlines highlight how stiffener geometry directly affects the target plate's ability to dissipate impact energy and reduce residual velocity.

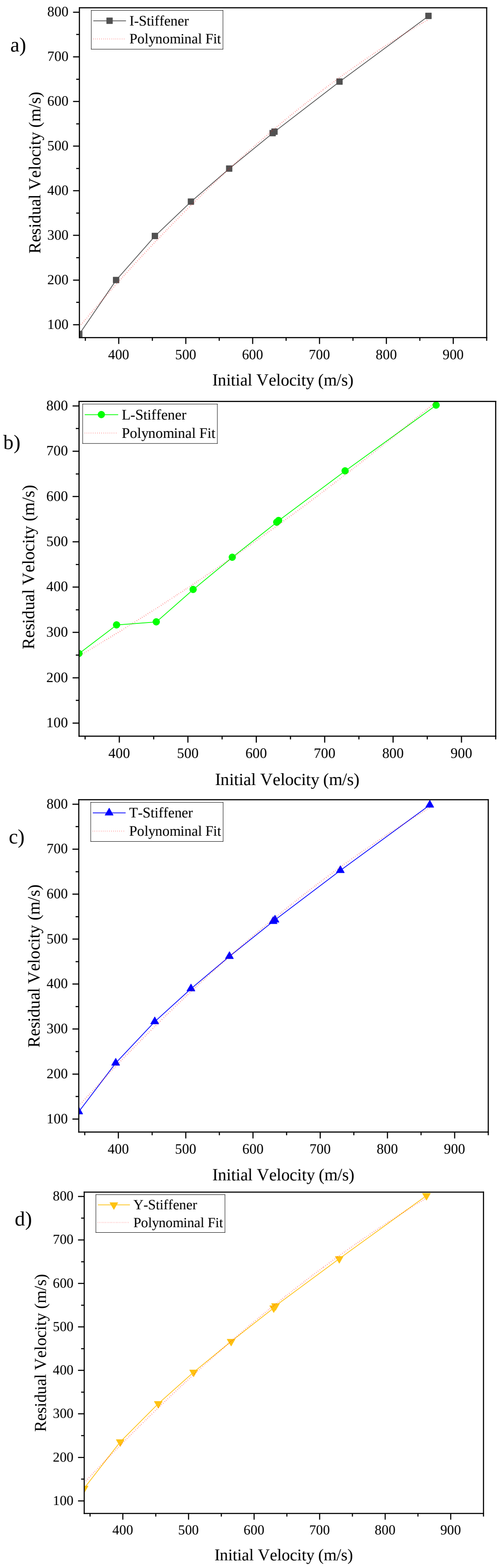

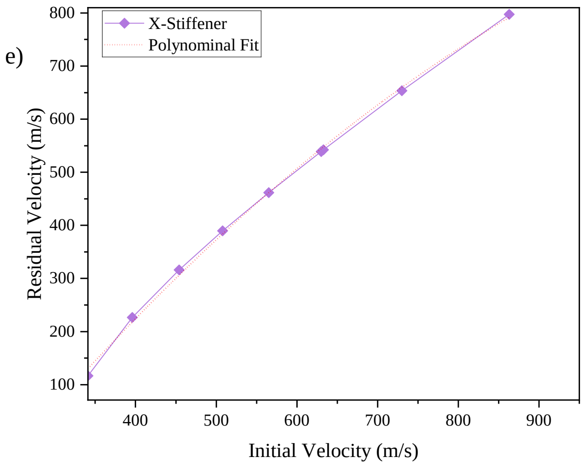


Figure 9. Trendline of the residual velocity graph of different stiffeners: a) I; b) L; c) T; d) Y; and e) X stiffener.

*Ballistic impact on target plate structure material*

The material utilised in the previous scenario is Al 6061-T561 for the target plate subjected to ballistic impact. This study performed simulations on the target plate using various material configurations to enhance protection against ballistic impact. The materials utilised includes Al 6061-T651, Al 6082-T6, Weldox 460E, and Armox 500T. This study aims to evaluate the performance of four materials under ballistic impact analysed in nine initial velocities, as detailed in Table 1. The target plate configuration featuring an I stiffener is selected due to its superior performance, as illustrated in Fig. 6. Figure 10 illustrates the simulation results of residual velocity generated by each material with nine initial bullet velocities. It can be found that Al 6082-T6 and Al 6061-T651 have elevated residual velocities throughout the spectrum of initial velocities, indicating enhanced energy retention and reduced deformation upon contact. On the other hand, Weldox 460E and Armox 500T have markedly reduced residual velocities, especially at elevated initial velocities, signifying enhanced energy dissipation and superior impact resistance. This comparison underscores the different material characteristics, with aluminium alloys emphasizing low energy retention, aside from steel materials such as Weldox 460E and Armox 500T, which provide superior energy absorption and penetration resistance, proving them suitable for protective applications.

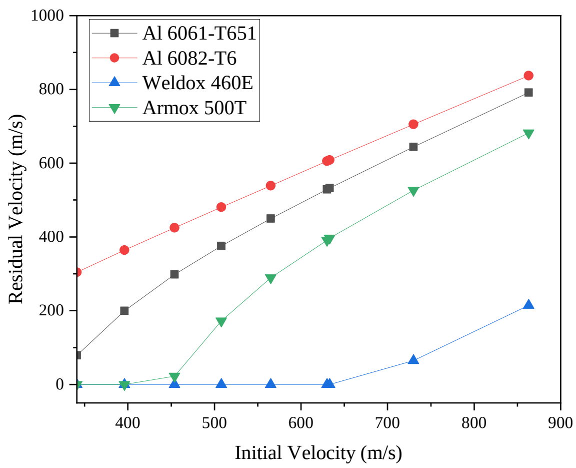


Figure 10. Comparison of residual velocity and initial velocity results using different material types.

The Von-Mises stress contours in Fig. 11 for the analysed materials reveal notable disparities in their capacity to endure and distribute stress under impact scenarios at different velocities. For Al 6061-T651, stress escalates with increasing impact velocities, exhibiting localised concentration in the impact zone at lower speeds and considerable deformation and fracture at elevated velocities when stress surpasses the yield strength. Al 6082 T6 has comparable behaviour, with stress concentration at the impact zone and marginally elevated stress levels, signifying reduced resistance to high-impact forces compared to Al 6061-T651. Conversely, the Weldox 460E exhibits significantly greater stress resilience with a more consistent stress distribution, even at elevated velocities. The steel material maintains its structural integrity at higher velocities, demonstrating enhanced impact resistance and energy absorption capabilities. Armox 500T, a high-strength steel, demonstrates superior stress tolerance compared to the other three materials. The stress is concentrated at the projectile interface, even at maximal velocities with no deformation, exhibiting its remarkable capacity to withstand high-velocity impacts, hence proving it more suitable for applications demanding enhanced impact resistance.

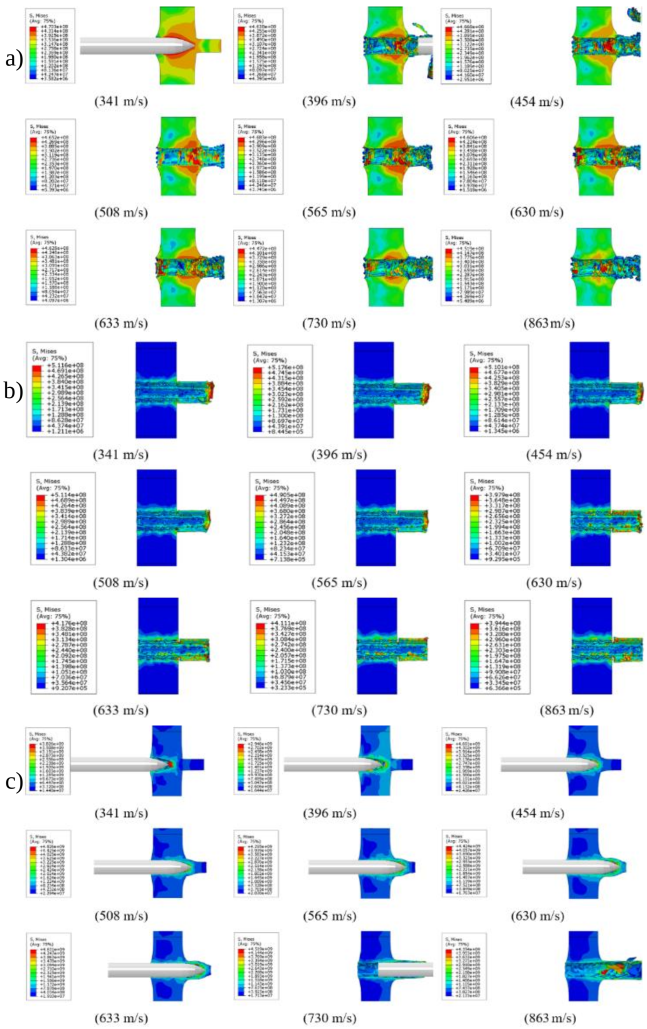

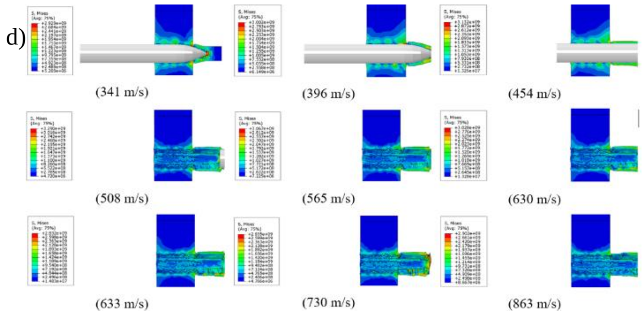

Figure 11. Von-Mises stress contours between material types: a) Al 6061-T651; b) Al 6082 T6; c) Weldox 460E; and d) Armox 500T.

## CONCLUSIONS

This numerical study has been carried out to assess the performance of stiffened target plate structures in absorbing impact energy from projectile penetration. The investigation involves analysing five stiffener profiles and four target plate materials under various initial projectile velocities using finite element analysis (FEA) software. The findings indicate that the I-stiffener demonstrates superior energy absorption capabilities, as evidenced by its ability to consistently reduce the projectile's velocity during penetration, resulting in the lowest residual velocity across the evaluated velocity range. In contrast, the L stiffener is less effective in mitigating projectile penetration, reflected by its higher residual velocity trendline.

Regarding material performance, the Weldox 460E and Armox 500T show significantly enhanced impact resistance, particularly at higher initial velocities. These materials exhibit superior energy dissipation, reducing residual velocities and highlighting their suitability for protective applications in structural design subjected to dynamic loading. Key areas for future investigation include repeated projectile impacts and the temperature effect on impact resistance, which can be investigated.

## ACKNOWLEDGMENTS

This work is supported by the ‘Rencana Anggaran dan Kerja Tahunan’ (RKAT) - Universitas Sebelas Maret Year 2024, under the Research Scheme of ‘Riset Kolaborasi Indonesia’ (RKI), with research grant/contract no. 285/UN27. 22/PT.01.03/2024. The authors highly acknowledge the support.

## REFERENCES

1. Kurtaran, H., Buyuk, M., Eskandarian, A. (2003), *Ballistic impact simulation of GT model vehicle door using finite element method*, Theor. Appl. Fract. Mech. 40(2): 113-121. doi: 10.1016/S0167-8442(03)00039-9
2. Rahman, N.A., Abdullah, S., Zamri, W.F.H., et al. (2016), *Ballistic limit of high-strength steel and Al7075-T6 multi-layered plates under 7.62-mm armour piercing projectile impact*, Lat. Am. J Solids Struct. 13(9): 1658-1676. doi: 10.1590/1679-78252657
3. Wang, Y., Lu, J., Liu, S., et al. (2021), *Behaviour of a novel stiffener-enhanced steel-concrete-steel sandwich beam subjected to impact loading*, Thin-Walled Struct. 165: 107989. doi: 10.1016/j.tws.2021.107989
4. Chung, K.Y.S., Nurick, G.N. (2005), *Experimental and numerical studies on the response of quadrangular stiffened plates. Part I: subjected to uniform blast load*, Int. J Impact Eng. 31 (1): 55-83. doi: 10.1016/j.ijimpeng.2003.09.048
5. Yong, C., Wang, Y., Tang, P., Hua, H. (2008), *Impact characteristics of stiffened plates penetrated by sub-ordnance velocity projectiles*, J Constr. Steel Res. 64(6): 634-643. doi: 10.1016/j.jcsr.2007.12.006
6. Kucharski, D.M.P., Pinto, V.T., Rocha, L.A.O., et al. (2022), *Geometric analysis by constructal design of stiffened steel plates under bending with transverse I-shaped or T-shaped stiffeners*, Facta Universitatis, Series: Mech. Eng. 20(3): 617-632. doi: 10.22190/FUME211016070K
7. Razak, N.S.A., Alias, A., Mohsan, N.M., Masjuki, S.A. (2023), *Numerical investigation of the failure of stiffened steel plates subjected to near-field blast loads*, J Fail. Anal. Prevent. 23(2): 569-591. doi: 10.1007/s11668-023-01628-5
8. Gan, L., Zong, Z., Lin, J., et al. (2022), *Influence of U-shaped stiffeners on the blast-resistance performance of steel plates*, J Constr. Steel Res. 188: 107046. doi: 10.1016/j.jcsr.2021.107046
9. Veeredhi, L.S.B., Ramana Rao, N.V. (2015), *Studies on the impact of explosion on blast resistant stiffened door structures*, J Inst. Eng. India: Ser. A, 96: 11-20. doi: 10.1007/s40030-014-0103-x
10. Kim, J.S., Kavak, H., Manzoor, U., Züfle, A. (2019), *Advancing simulation experimentation capabilities with runtime interventions*, Spring Simulation Conference (SpringSim), Tucson, AZ, USA, 2019, pp.1-11, doi: 10.23919/SpringSim.2019.8732869
11. Jones, N., Kim, S.B., Li, Q.M. (1997), *Response and failure of ductile circular plates struck by a mass*. J Press. Ves. Technol., Trans. ASME, 119(3): 332-342. doi: 10.1115/1.2842313
12. Prabowo, A.R., Laksono, F.B., Sohn, J.M. (2020), *Investigation of structural performance subjected to impact loading using finite element approach: case of ship-container collision*, Curv. Layer. Struct. 7(1): 17-28. doi: 10.1515/cls-2020-0002
13. Zahari, R., Pillai, J.R., Ordys, A., et al. (2018), *Ballistic impact analysis of double-layered metal plates*, IOP Conf. Ser.: Mater. Sci. Eng. 405: 012012. doi: 10.1088/1757-899X/405/1/012012
14. Singh, D.K., Banerjee, A., Datta, D. (2024), *Ballistic resistance of ceramic and metal target plates impacted against different projectile’s nose shape: A numerical investigation*, Mech. Adv. Mater. Struct. 1-13. doi: 10.1080/15376494.2024.2400586
15. Gruben, G., Sølvernes, S., Berstad, T., et al. (2017), *Low-velocity impact behaviour and failure of stiffened steel plates*, Marine Struct. 54: 73-91. doi: 10.1016/j.marstruc.2017.03.005
16. Singh, P.K., Kumar, M. (2024), *Finite element analysis of the ballistic performance of monolithic and double-layered plates subjected to deformable projectiles*, Mech. Adv. Mater. Struct. 31(26): 7976-7990. doi: 10.1080/15376494.2023.2253454
17. Ranaweera, P., Bambach, M.R., Weerasinghe, D., Mohotti, D. (2023), *Ballistic impact response of monolithic steel and tri-metallic steel-titanium-aluminium armour to nonrigid NATO FMJ M80 projectiles*, Thin-Walled Struct. 182(Part A): 110200. doi: 10.1016/j.tws.2022.110200
18. Prabowo, A.R., Byeon, J.H., Cho, H.J., et al. (2018), *Impact phenomena assessment: Part I-Structural performance of a tanker subjected to ship grounding at the Arctic*, MATEC Web Conf. 159: 02061. doi: 10.1051/matecconf/201815902061
19. DeMange, J.J., Prakash, V., Pereira, J.M. (2009), *Effects of material microstructure on blunt projectile penetration of a nickel-based super alloy*, Int. J Impact Eng. 36(8): 1027-1043. doi: 10.1016/j.ijimpeng.2009.01.007
20. Liu, B., Villavicencio, R., Guedes Soares, C. (2013), *Experimental and numerical plastic response and failure of laterally impacted rectangular plates*, J Offshore Mech. Arct. Eng. 135 (4): 041602. doi: 10.1115/1.4024274

21. Grytten, F., Børvik, T., Hopperstad, O.S., Langseth, M. (2009), *Low velocity perforation of AA5083-H116 aluminium plates*, Int. J Impact Eng. 36(4): 597-610. doi: 10.1016/j.ijimpeng.2008.09.002
22. Prabowo, A.R., Muttaqie, T., Sohn, J.M., Bae, D.M. (2018), *Nonlinear analysis of inter-island RoRo under impact: effects of selected collision's parameters on the crashworthy double-side structures*, J Braz. Soc. Mech. Sci. Eng. 40: 248. doi: 10.1007/s40430-018-1169-6
23. Wang, Y., Wang, Z., Liang, S., et al. (2023), *Experimental and numerical study on the failure modes of ship stiffened plate structure under projectile perforation*, Int. J Impact Eng. 178: 104590. doi: 10.1016/j.ijimpeng.2023.104590
24. Zhan, T., Li, J., Lv, S., Chen, Z. (2016), *Residual velocity for the truncated ogival-nose projectile into stiffened plates*, Ships Offshore Struct. 11(6): 636-644. doi: 10.1080/17445302.2015.1041441
25. Greenhalgh, E., Bishop, S.M., Bray, D., et al. (1996), *Characterisation of impact damage in skin-stringer composite structures*, Compos. Struct. 36(3-4): 187-207. doi: 10.1016/S0263-8223(96)00077-3
26. Greenhalgh, E., Meeks, C., Clarke, A., Thatcher, J. (2003), *The effect of defects on the performance of post-buckled CFRP stringer-stiffened panels*, Compos. Part A: Appl. Sci. Manuf. 34(7): 623-633. doi: 10.1016/S1359-835X(03)00098-8
27. Greenhalgh, E., Garcia, M.H. (2004), *Fracture mechanisms and failure processes at stiffener run-outs in polymer matrix composite stiffened elements*, Compos. Part A: Appl. Sci. Manuf. 35 (12): 1447-1458. doi: 10.1016/j.compositesa.2004.05.006
28. Greenhalgh, E., Hiley, M. (2003), *The assessment of novel materials and processes for the impact tolerant design of stiffened composite aerospace structures*, Compos. Part A: Appl. Sci. Manuf. 34(2): 151-161. doi: 10.1016/S1359-835X(02)00188-4
29. Wang, Y., Wang, Z., Yao, X., Yang, N. (2024), *Effect of Lode angle in predicting the behaviour of stiffened 921A steel target plates in ballistic impact by truncated ogive projectiles*, Int. J Impact Eng. 185: 104841. doi: 10.1016/j.ijimpeng.2023.104841
30. Prabowo, A.R., Ridwan, R., Tuswan, T., et al. (2024), *Crushing resistance on the metal-based plate under impact loading: A systematic study on the indenter radius influence in grounding accident*, Appl Eng Sci. 18: 100177. doi: 10.1016/j.apples.2024.100177
31. Ansori, D.T.A., Prabowo, A.R., Muttaqie, T., et al. (2022), *Investigation of honeycomb sandwich panel structure using aluminum alloy (AL6XN) material under blast loading*, Civ. Eng J, 8(5): 1046-1068. doi: 10.28991/CEJ-2022-08-05-014
32. Langdon, G.S., Yuen, S.C.K., Nurick, G.N. (2005), *Experimental and numerical studies on the response of quadrangular stiffened plates. Part II: localised blast loading*, Int. J Impact Eng. 31(1): 85-111. doi: 10.1016/j.ijimpeng.2003.09.050
33. Gan, L., Zong, Z. (2024), *Damage assessment of fixed U-shaped stiffeners stiffened square plates subjected to close-in explosions*, Eng. Struct. 319: 118905. doi: 10.1016/j.engstruct.2024.118905
34. Piekutowski, A.J., Forrestal, M.J., Poormon, K.L., Warren, T.L. (1996), *Perforation of aluminum plates with ogive-nose steel rods at normal and oblique impacts*, Int. J Impact Eng. 18(7-8): 877-887. doi: 10.1016/S0734-743X(96)00011-5
35. Deng, Y., Zhang, Y., Zeng, X., Yang, Y. (2020), *Dynamic mechanical properties and modification of fracture criteria of 6061-T651 aluminum alloy*, Jixie Gongcheng Xuebao/Chinese J Mech. Eng. 56(18): 81-91. doi: 10.3901/JME.2020.18.081
36. Gopi, S., Mohan, D.G. (2021), *Evaluating the welding pulses of various tool profiles in single-pass friction stir welding of 6082-T6 aluminium alloy*, J Weld. Join. 39(3): 284-294. doi: 10.5781/JWJ.2021.39.3.7
37. Saxena, A., Kumaraswamy, A., Kotkunde, N., Suresh, K. (2019), *Constitutive modeling of high-temperature flow stress of armor steel in ballistic applications: A comparative study*. J Mater. Eng. Perform. 28: 6505-6513. doi: 10.1007/s11665-019-04337-z
38. Wang, X., Shi, J. (2013), *Validation of Johnson-Cook plasticity and damage model using impact experiment*, Int J Impact Eng. 60: 67-75. doi: 10.1016/j.ijimpeng.2013.04.010
39. Lazarević, M., Živković, B., Bajić, D., et al. (2023), *Properties of aluminium-steel plates explosively welded using amonex*, Stuct. Integr. Life, 23(2): 141-146.
40. Ridwan, R., Sudarno, S., Nubli, H., et al. (2023), *Numerical analysis of openings in stiffeners under impact loading: Investigating structural response and failure behavior*, Mekanika: Majalah Ilmiah Mekanika, 22(2): 115-125. doi: 10.20961/mekanika.v22i2.76774
41. Dinulović, M., Grbović, A., Adžić, V., Alarafati, H. (2023), *Composite plates with nomex honeycomb core modelling for dynamic integrity at the mesoscale level*, Stuct. Integr. Life, 23 (2): 147-153.
42. Mohammad, Z., Gupta, P.K., Baqi, A. (2020), *Experimental and numerical investigations on the behavior of thin metallic plate targets subjected to ballistic impact*, Int. J Impact Eng. 146: 103717. doi: 10.1016/j.ijimpeng.2020.103717
43. Wiranto, I.B., Saraswati, S.O., Alfikri, I.R., et al. (2024), *Effect of boundary condition on numerical study of UAV composite skin panels under dynamic impact loading*, Mekanika: Majalah Ilmiah Mekanika, 23(1): 22-32. doi: 10.20961/mekanika.v23i1.77875
44. Belamri, S., Lebbal, H., Yahiaou, T., et al. (2023), *Experimental and numerical determination of defects in rectangular plates with vibration analysis method*, Stuct. Integr. Life, 23(2): 173-178.
45. Zhang, Y., Dong, H., Liang, K., Huang, Y. (2021), *Impact simulation and ballistic analysis of $B_4C$ composite armour based on target plate tests*, Cer. Int. 47(7, Part A): 10035-10049. doi: 10.1016/j.ceramint.2020.12.150
46. Carvalho, H., Ridwan, R., Sudarno, S., et al. (2023), *Failure criteria in crashworthiness analysis of ship collision and grounding using FEA: milestone and development*, Mekanika: Majalah Ilmiah Mekanika, 22(1): 30-39. doi: 10.20961/mekanika.v22i1.70959
47. Verreault, J. (2015), *Analytical and numerical description of the PELE fragmentation upon impact with thin target plates*, Int. J Impact Eng. 76: 196-206. doi: 10.1016/j.ijimpeng.2014.09.012
48. Zhang, Z.L., Feng, D.L., Ma, T., Liu, M.B. (2019), *Predicting the damage on a target plate produced by hypervelocity impact using a decoupled finite particle method*, Eng Anal. Bound. Elem. 98: 110-125. doi: 10.1016/j.enganabound.2018.10.012